Very sensitive fiber Bragg grating accelerometer using transverse forces with an easy over-range protection and low cross axial sensitivity

Kuo Li,[1,*] Tommy H. T. Chan,[1] Man Hong Yau,[1] Theanh Nguyen,[1] David P. Thambiratnam,[1] and Hwa Yaw Tam[2]

[1]Civil Engineering and Built Environment, Queensland University of Technology, Brisbane 4000, Australia

[2]Photonic Research Centre, The Hong Kong Polytechnic University, Hong Kong, China

*Corresponding author: tolikuo@gmail.com

Received 14 May 2013; revised 9 July 2013; accepted 30 July 2013;
posted 1 August 2013 (Doc. ID 190502); published 30 August 2013

The first fiber Bragg grating (FBG) accelerometer using direct transverse forces is demonstrated by fixing the FBG by its two ends and placing a transversely moving inertial object at its middle. It is very sensitive because a lightly stretched FBG is more sensitive to transverse forces than axial forces. Its resonant frequency and static sensitivity are analyzed by the classic spring-mass theory, assuming the axial force changes little. The experiments show that the theory can be modified for cases where the assumption does not hold. The resonant frequency can be modified by a linear relationship experimentally achieved, and the static sensitivity by an alternative method proposed. The principles of the over-range protection and low cross axial sensitivity are achieved by limiting the movement of the FBG and were validated experimentally. The sensitivities 1.333 and 0.634 nm/g were experimentally achieved by 5.29 and 2.83 gram inertial objects at 10 Hz from 0.1 to 0.4 g ($g = 9.8 \times$ m/s^2), respectively, and their resonant frequencies were around 25 Hz. Their theoretical static sensitivities and resonant frequencies found by the modifications are 1.188 nm/g and 26.81 Hz for the 5.29 gram one and 0.784 nm/g and 29.04 Hz for the 2.83 gram one, respectively.

OCIS codes: (060.3735) Fiber Bragg gratings; (060.2370) Fiber optics sensors.
http://dx.doi.org/10.1364/AO.52.006401

1. Introduction

Fiber Bragg grating (FBG) sensors are well suited for many fields such as structural health monitoring [1,2] and seismic monitoring [3,4] because of their intrinsic advantages of frequency modulation, ease of multiplexing, and strong immunity to electromagnetic interference [5]. FBG is inherently sensitive to strain and temperature. Modulating its strain can measure acceleration [3–17], strain and displacement [18,19], inclination [20,21], temperature [22,23], and so on. We demonstrated that its strain is more sensitive to transverse forces than axial forces [24]. Here we demonstrate a very sensitive FBG accelerometer using transverse forces with an easy over-range protection and low cross axial sensitivity.

The theory of accelerometers is briefly reviewed, and the resonant frequency, static sensitivity, and over-range protection of this FBG accelerometer are analyzed. Two FBG accelerometers were manufactured, and their designs enable them to be insensitive to the other two orthogonal directions. They were tested at 0.1–0.4 g and 5–35 Hz. Because their experimental resonant frequencies disagree with their theoretical ones, another investigation experiment was carried out. A linear relationship was found to modify the theoretical resonant frequency. Because their experimental static sensitivities disagree with their theoretical ones, an alternative method for

1559-128X/13/256401-10$15.00/0

calculating the theoretical static sensitivity was proposed. The over-range protection and low cross axial sensitivity were experimentally validated.

Over-range protection is very important for accelerometers and usually determines its commercialization [25]. With a high sensitivity and easy over-range protection, this FBG accelerometer has the potential to be commercialized.

2. Theory

In an undamped, free-vibrated spring-mass system as shown in Fig. 1(a),

$$F = ma = m\frac{d^2x}{dt^2}, \tag{1}$$

$$F = -kx, \tag{2}$$

where F, m, a, x, t, and k are the net force applied on the inertial object, its mass, acceleration, displacement from equilibrium, time, and the spring constant, respectively.

From Eqs. (1) and (2),

$$\frac{d^2x}{dt^2} + \frac{k}{m}x = 0, \tag{3}$$

$$x = \cos\sqrt{k/m}t = \cos\,\omega_0 t = \cos\,2\pi f_0 t, \tag{4}$$

where ω_0 and f_0 are its resonant frequency in radians per second and hertz, respectively.

In an undamped forced system as shown in Fig. 1(b), assume that its displacement $z = z_0\cos\omega t$, where z_0 and ω are its amplitude and angular frequency. So,

$$F = ma = m\frac{d^2x}{dt^2} = -k(x-z) = -k(x - z_0\cos\omega t),$$
$$\frac{d^2x}{dt^2} + \frac{k}{m}x = \frac{k}{m}z_0\cos\omega t \rightarrow \frac{d^2x}{dt^2} + \omega_0^2 x = \omega_0^2 z_0\cos\omega t. \tag{5}$$

Substituting its steady-state solution $x = x_0\cos\omega t$ into Eq. (5), its amplitude is

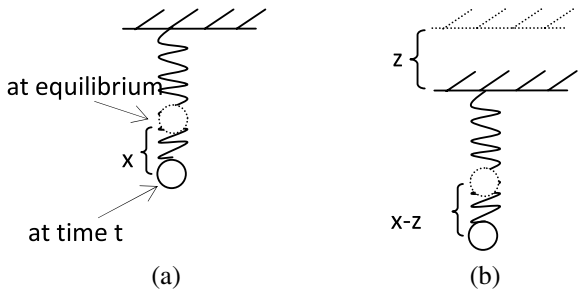

Fig. 1. Diagrams of an undamped (a) free-vibrated and (b) forced spring-mass system.

$$x_0 = \frac{\omega_0^2}{\omega_0^2 - \omega^2}z_0. \tag{6}$$

The acceleration of the inertial object (measured) is

$$a = \frac{d^2x}{dt^2} = -x_0\omega^2\cos\omega t. \tag{7}$$

The acceleration of the system (measurand) is

$$a' = \frac{d^2z}{dt^2} = -z_0\omega^2\cos\omega t. \tag{8}$$

So,

$$\frac{a}{a'} = \frac{\omega_0^2}{\omega_0^2 - \omega^2}. \tag{9}$$

Figure 2 further illustrates this relationship, which is achieved by a numerical simulation method as below. First, ω/ω_0 is assigned as 0.001, and its corresponding a/a' is found by Eq. (9). Second, ω/ω_0 is increased by 0.001 each time, and its corresponding a/a' is found. Finally, they are plotted together. The measured acceleration is the same as the measurand at static (0 Hz), but the measured will have an increasing systematic error as the frequency increases from 0 Hz to its resonant frequency. Industrially, the measurement ranges with ±5%, ±10%, and ±3 dB errors are usually given as below ~20%, ~30%, and ~50% of the resonant frequency [26]. Therefore, the resonant frequency of an accelerometer determines its measurement frequency range with a rather constant sensitivity. The higher its resonant frequency, the wider its measurement frequency range.

From Eq. (5), its static sensitivity in terms of the relative displacement between its inertial object and shell, being the change in its spring length from that at equilibrium, is

$$\left|\frac{x-z}{a}\right| = \frac{m}{K} = \frac{1}{\omega_0^2}. \tag{10}$$

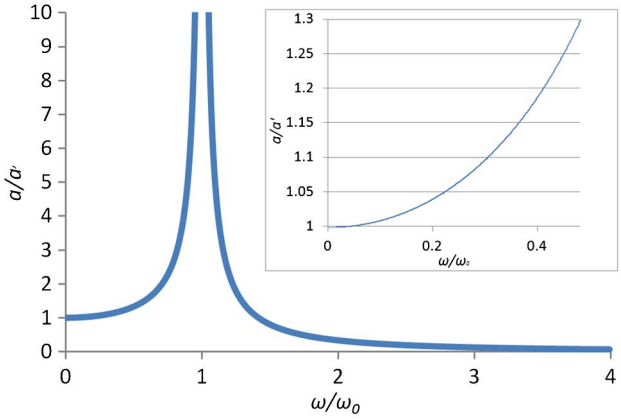

Fig. 2. Systematic errors of the measured acceleration at different frequencies.

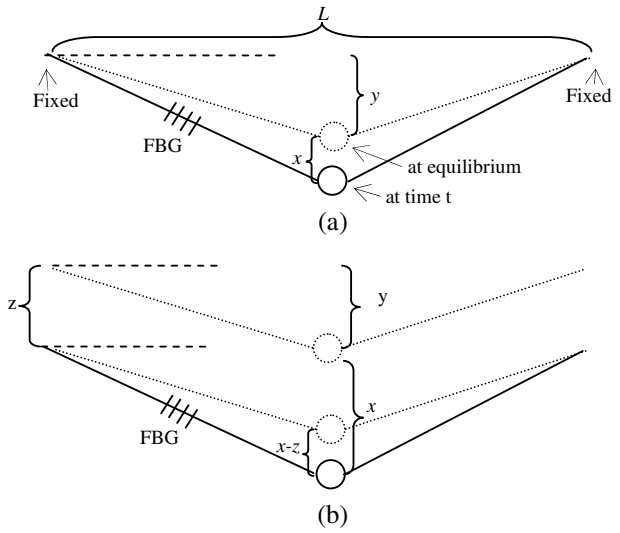

Fig. 3. Diagrams of the proposed FBG accelerometer in undamped (a) free and (b) forced vibrations.

The higher its resonant frequency, the lower its sensitivity. So there is a trade-off between its measurement frequency range and sensitivity. Accelerometers with high sensitivities are important in seismic monitoring [3] and space projects [27]. The measurement frequency range can be widen a little by introducing proper damping [17,28].

Figure 3 shows the principle of the proposed accelerometer. Assume that an inertial object was hung in the middle of a string with a length L, and the axial force at equilibrium F_e changes little. Assume that the displacement due to gravity is y, while $y = 0$ if there is no gravity in the measured direction.

In an undamped free-vibrated system as shown in Fig. 3(a),

$$ma = -2F_e\frac{x+y}{L/2} + mg = -4F_e\frac{x}{L}. \tag{11}$$

Its resonant frequency is

$$f_0 = \sqrt{F_e/(mL)}/\pi. \tag{12}$$

In an undamped forced system as shown in Fig. 3(b),

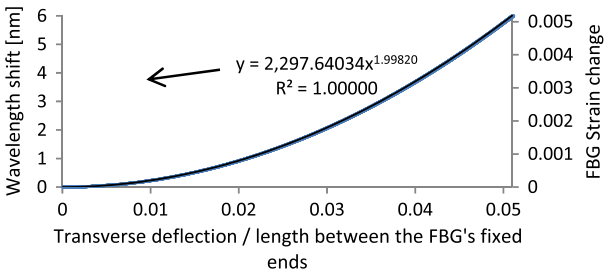

Fig. 4. Relationship between an FBG's resonant wavelength shift/strain change and the transverse deflection at its middle.

$$ma = -2F_e\frac{x-z+y}{L/2} + mg = -4F_e\frac{x-z}{L}. \tag{13}$$

Substituting its steady-state solution $x = x_0\cos\omega t$ into Eq. (13), its amplitude is still $(\omega_0^2/\omega_0^2 - \omega^2)z_0$. So Eq. (9) and Fig. 2 still apply.

Its static sensitivity in terms of the relative displacement, being the change in the transverse deflection of its FBG from that at equilibrium, is still $1/\omega_0^2$. The transverse deflection and strain change of the FBG have a simple triangular relationship. Figure 4 shows this relationship by the ratio of the transverse deflection to the length (RTDL) between the FBG's fixed ends, which is $(y+x)/L$ in Fig. 3(a) and $(y+x-z)/L$ in Fig. 3(b). It is achieved by the

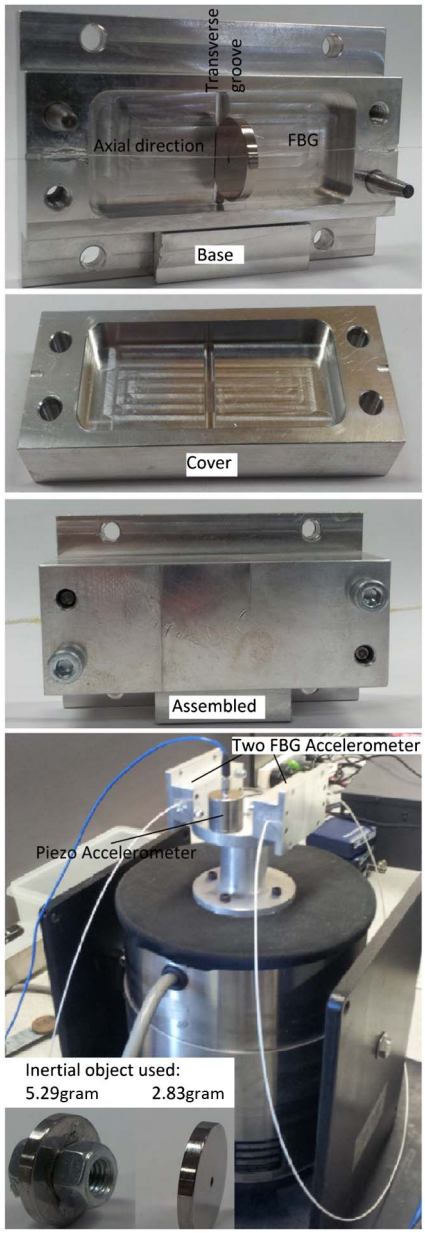

Fig. 5. Design and experimental setup of the proposed FBG accelerometer.

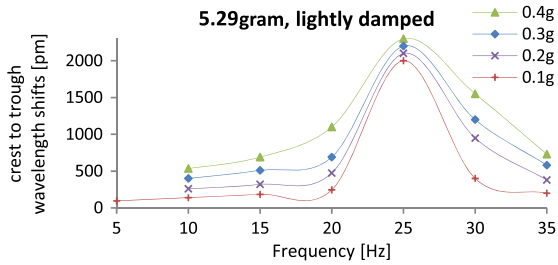

(a)

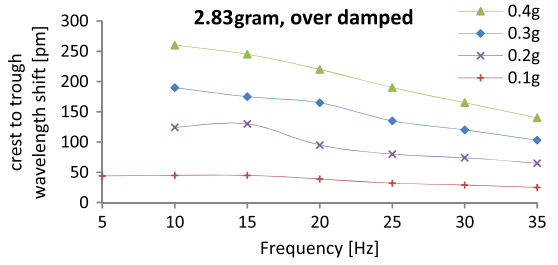

(b)

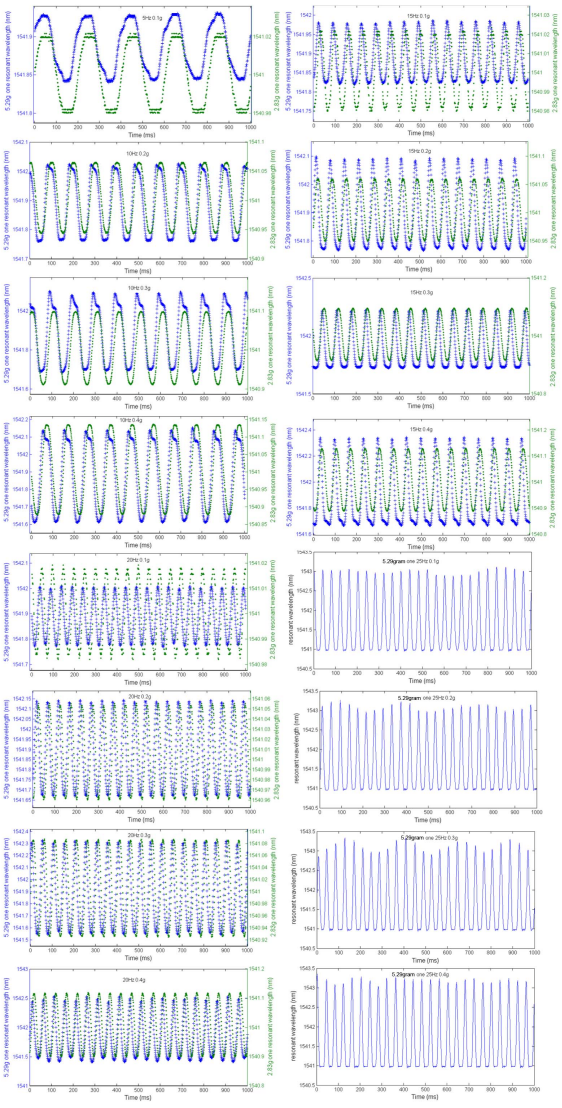

(c)

Fig. 6. Frequency responses of the (a) 5.29 gram and (b) 2.83 gram accelerometers, and (c) some of their original records.

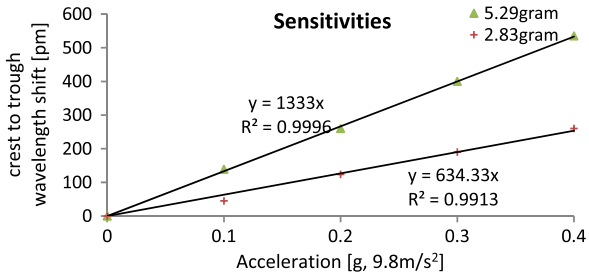

Fig. 7. Experimental sensitivities of the 5.29 and 2.83 gram accelerometers.

numerical simulation method used for Fig. 2. The resonant wavelength shift is converted by using the experimental results ($\Delta\lambda = 1159.02\Delta\varepsilon$) [24]. In this way, its sensitivity in terms of its resonant wavelength shift can be found.

Over-range protection can be achieved by limiting RTDL to confine the FBG's strain change. An FBG may break when its strain change is much larger than 0.005, which corresponds to ~5% in RTDL and 6 nm in its resonant wavelength shift.

3. Experiments and Discussion

Figure 5 shows the design and experimental setup of the proposed FBG accelerometer. The transverse grooves are 21 mm in length, which confines a Φ15 mm cylinder with a Φ1 mm hole at its center to only move transversely to the FBG. Also, this accelerometer is nonsensitive to the other two orthogonal directions, because (1) the cylinder is confined by the grooves and shells and (2) the movements of the cylinder in the other two orthogonal directions are about 0.2 mm and will scarcely pull the FBG because the FBG is in the Φ1 mm hole of the cylinder. For the position accuracy between the base and cover, two rims were used. Two FBG accelerometers with the same size ($L = 50$ mm), but different inertial masses (5.29 and 2.83 gram) were made and tested. Their Bragg gratings were manufactured on bending insensitive fibers (Silibend G.657.B, Silitec Fibers Ltd.) by using phase masks, ~10 mm in length, ~2 nm of 3 dB bandwidth, and ~90% of reflectivity. The FBG of the 5.29 gram one (free-state wavelength: 1541.05 nm) were prestretched 0.03 nm in terms of its resonant wavelength shift, while that

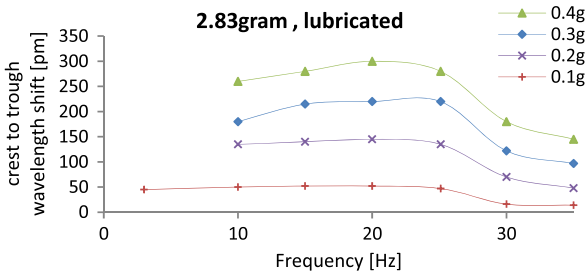

Fig. 8. Frequency responses of the 2.83 gram accelerometer after being lubricated.

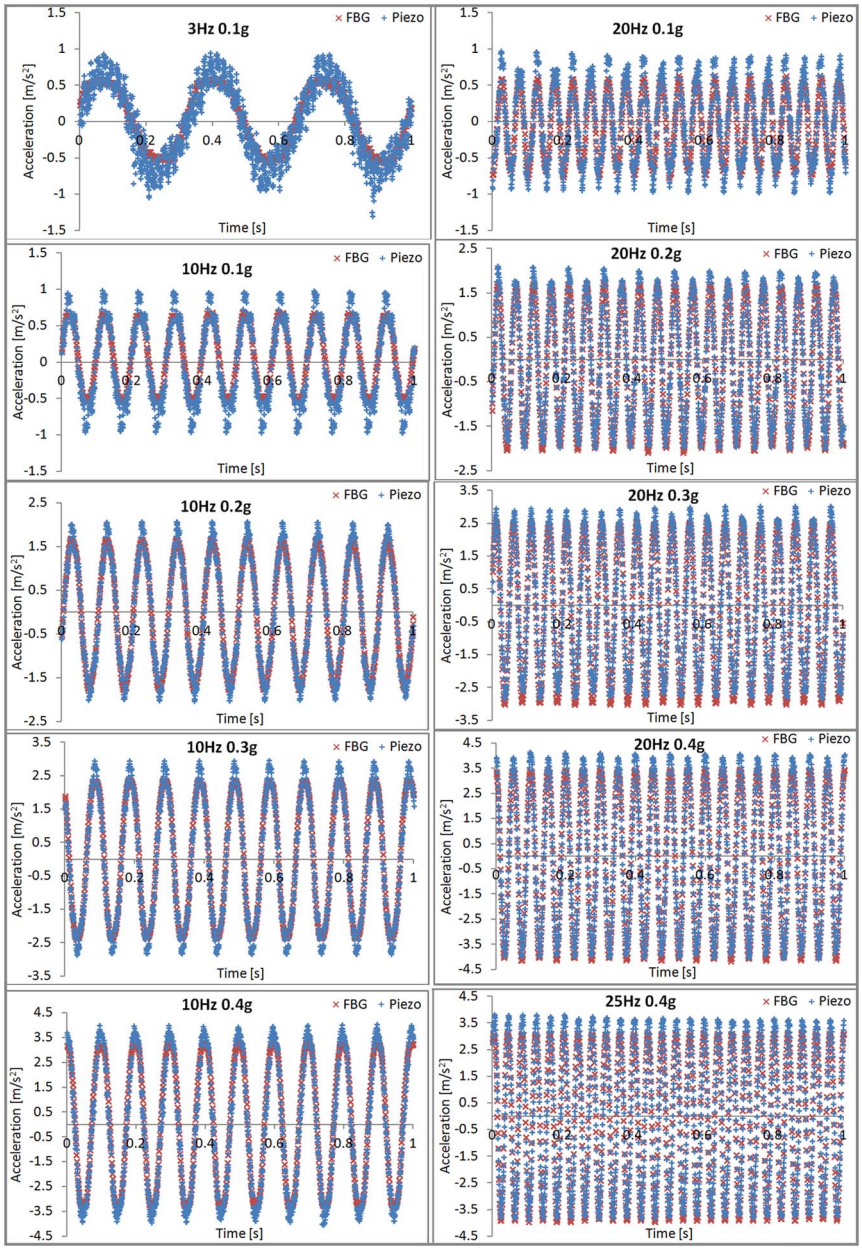

Fig. 9. Comparisons between the accelerations observed by the piezo accelerometer and the lubricated 2.83 gram one.

of the 2.83 gram one was stretched 0.1 nm (free state: 1540.40 nm). The ends of the FBGs were fixed by super glue (Loctite Ltd.). A wavelength interrogator (SM130, Micronoptics Ltd.) working at 1000 Hz with a repeatability of 1 pm was used. A calibrated PCB 393B piezo accelerometer working at 1653 Hz with a sensitivity 10 V/g and measurement range [–0.5 g, 0.5 g] was used as gauge. Sine waves were generated by an EZ digital FG-7002C sweep/function generator, amplified by a Crown CE2000 amplifier, and fed to a shaker (VG 100-4, Aurora, OH. 44202). The acceleration of the shaker was monitored by a piezo accelerometer and tuned to test the FBG accelerometers. The shaker was only able to provide 0.4 g acceleration starting from near 10 Hz, because the maximum acceleration that a shaker can provide decreases as its vibration frequency decreases.

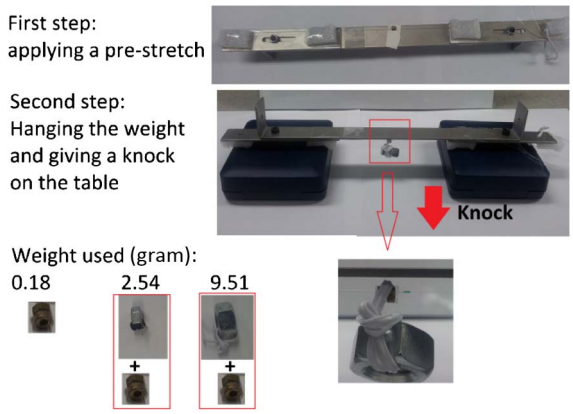

Fig. 10. Setup of the resonant frequency investigation experiment.

Figures 6(a) and 6(b) show their frequency responses by the estimated averages of the original records, and also show that the 5.29 gram one was lightly damped and the 2.83 gram one was overdamped. Figure 6(c) shows some of their experimental records. Because the 5.29 gram one was constituted by gluing two small nuts on a similar 2.83 gram cylinder, their frictions, working as damping, were similar. However, at the same acceleration, the force from the 5.29 gram one was nearly twice that of the other, which resulted in these different damping results. Figure 7 shows their sensitivities at 10 Hz, 1.333 nm/g for the 5.29 gram one and 0.634 nm/g for the 2.83 gram one.

The 2.83 gram one was lubricated to reduce the friction and then tested again. Figure 8 shows its overall frequency responses. Its sensitivity at 10 Hz changed little, although the change in damping shows that the friction reduced. Figure 9 shows the comparisons between the accelerations observed by this one and the piezo one, and their positive directions are upward. Its accelerations were achieved by first converting its observed wavelengths to the transverse forces [24] and then deducting the transverse force at equilibrium from them to find the net forces applied, and finally dividing by the mass to find its accelerations.

Figures 6(a), 6(b), and 8 show that their experimental resonant frequencies were around 25 Hz, which

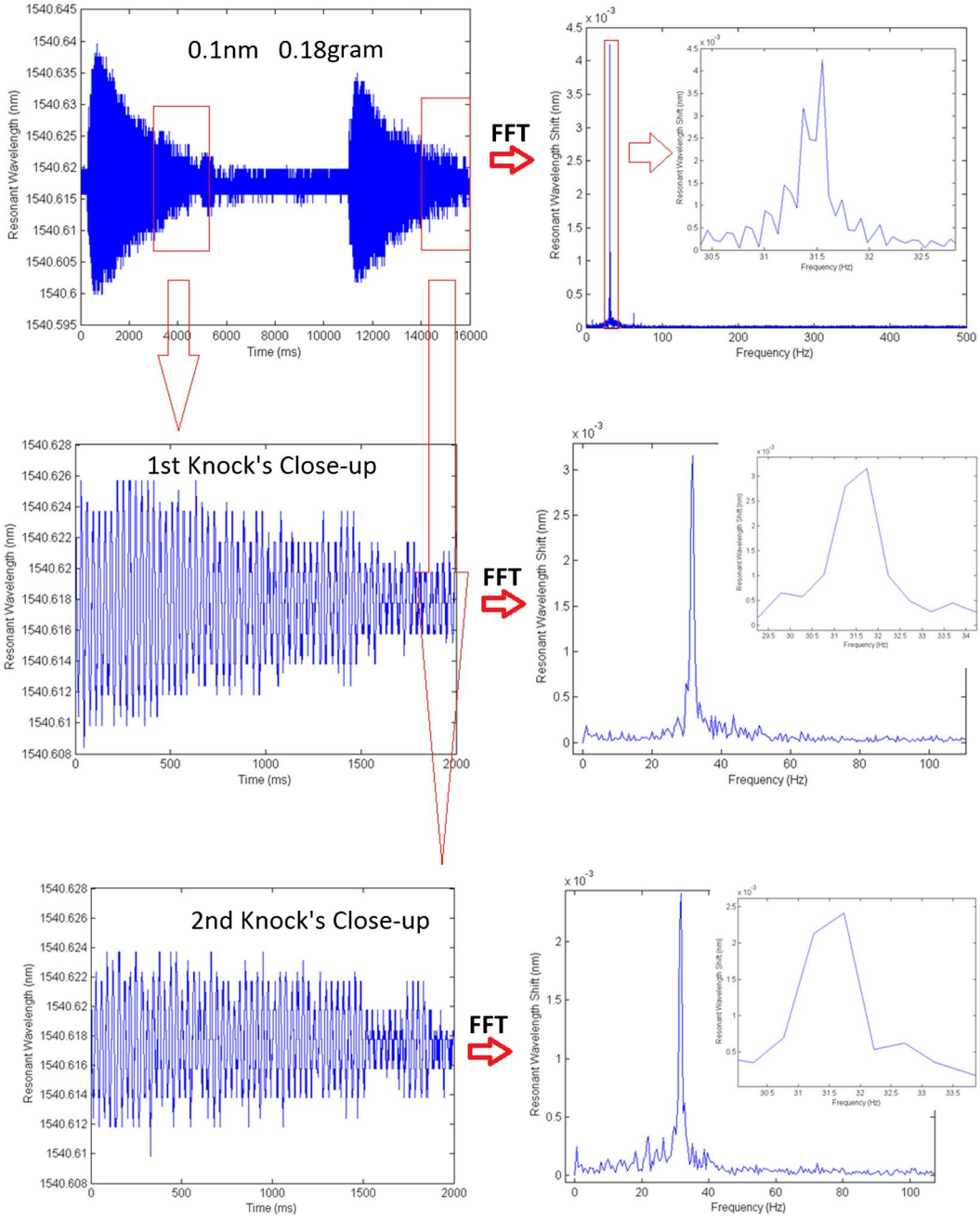

Fig. 11. Time domain records and their FFT at 0.1 nm prestretch, 0.18 gram weight, and two knocks.

Table 1. Resonant Frequency at the Different Prestretches and Weights of the Inertial Objects

Prestretch (nm)	Inertial Object (gram)	Stretch at Equilibrium (nm)	Theoretical Resonant Frequency (Hz)	Experimental (Hz)	Percentage Error	Ratio of the Stretch by the Weight to the Total Stretch
0.1	0.18	0.15	25.2	31.5	0.25	0.33
	2.54	0.58	13.2	21.6	0.64	0.83
	9.51	1.35	10.4	17.4	0.67	0.93
0.69	0.18	0.74	56.0	57.4	0.03	0.07
	2.54	0.93	16.7	20.1	0.20	0.26
	9.51	1.61	11.4	15.9	0.40	0.57
1.65	0.18	1.67	84.1	85.6	0.02	0.01
	2.54	1.73	22.8	23.7	0.04	0.05
	9.51	2.16	13.2	15.5	0.18	0.24
2.34	0.18	2.38	100.4	101.5	0.01	0.02
	2.54	2.42	26.9	27.2	0.01	0.03
	9.51	2.69	14.7	16.2	0.10	0.13
3.26	2.54	3.32	31.6	31.6	0.00	0.02
	9.51	3.49	16.7	17	0.02	0.07

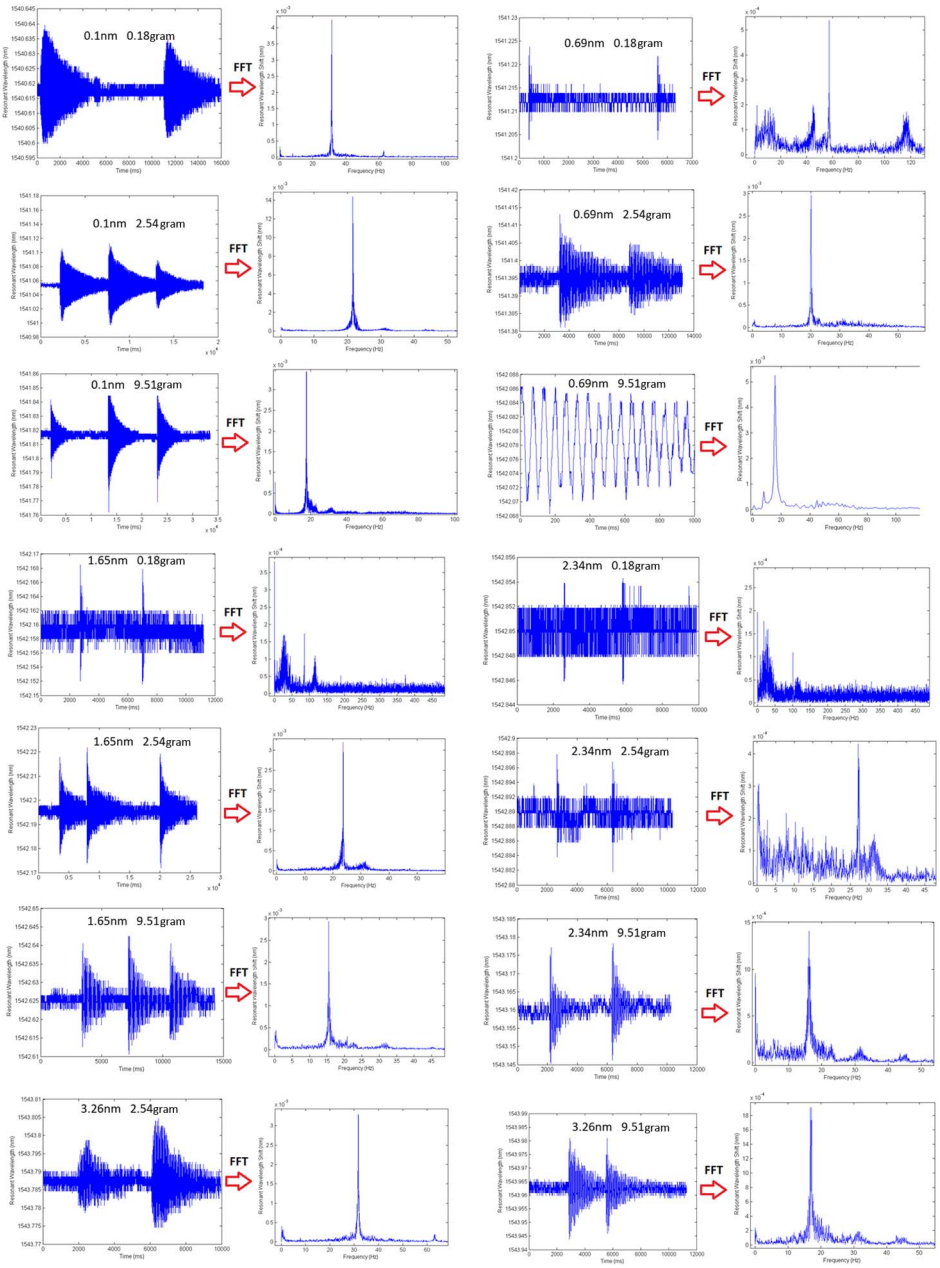

Fig. 12. Resonant frequency at the different prestretches of the FBG and weights of the inertial object.

were evidently higher than the theoretical ones, 15.65 Hz for the 5.29 gram one (0.85 nm stretched at equilibrium, $F_e = (0.85/1.33)$ N from the experimental results [24], and $f_0 = \sqrt{(F_e/mL)}/\pi = \sqrt{0.85/1.33/(0.00529 * 0.05)}/3.1416$ Hz $= 15.65$ Hz) and 17.97 Hz for the 2.83 gram one (0.6 nm stretched at equilibrium, $\sqrt{0.6/1.33/(0.00283 * 0.05)}/3.1416$ Hz $= 17.97$ Hz). To further investigate it, we used a setup shown in Fig. 10, which can tune the prestretch of the FBG (free state: 1540.47 nm) by moving the right-side metal strips with a slot thereon [22]. The length between the FBG's fixed ends was 100 mm. After applying a prestretch to the FBG, an object was hung at the center of the FBG. Then, the table was knocked once to incite the resonant vibration. Figure 11 shows the time domain records and their fast Fourier transform (FFT) when the FBG was prestretched 0.1 nm, a 0.18 gram weight was hung afterward, and two knocks were given. The overall records and two of its partials incited by the two knocks agree well with the resonant frequency. This method was used to analyze the resonant frequency of this setup, because the consistency of the resonant frequencies achieved under different knocks has been excellent throughout this experiment. Table 1 and Fig. 12 show the resonant frequency at the different prestretches and weights of the inertial objects. The percentage error and the ratio in Table 1 have a linear relationship, as shown in Fig. 13. The resonant frequency agrees with the theoretical value well when the stretch by the weight is negligible. But its deviation from the theoretical value increases with the ratio, which should be because the assumption that the axial force changes little does not hold there.

Therefore, the theoretical frequencies of the 5.29 and 2.83 gram ones can be modified as $15.65 * (1 + ((0.85 - 0.03)/0.85) * 0.7395) = 26.81$ Hz and $17.97 * (1 + ((0.6 - 0.1)/0.6) * 0.7395) = 29.04$ Hz. The above knock incitation method was also applied to them, but their consistencies were not good, probably due to the frictions. Figure 14 shows the records of the 5.29 gram one under five knocks.

Similarly, their static sensitivities found in the classic method, 3.530 nm/g for the 5.29 gram one and 2.090 nm/g for the 2.83 gram one, disagree with the experiments. They are found as below. First, the RTDLs at equilibrium are found by the inverse function of the equation in Fig. 4 ($y = 0.02079x^{0.50045}$, achieved by the numerical simulation method), 1.88% for the 5.29 gram one (0.82 nm stretched by the weight, $0.02079 * 0.82^{0.50045} = 1.88\%$), and 1.47% for the 2.83 gram one (0.5 nm stretched by the weight). Second, RTDLs made by 0.001 g are found by $0.001 * 9.8 * (1/\omega_0^2)/L$, 0.00203% for the 5.29 gram one and 0.00154% for the 2.83 gram one. So, at 0.001 g, the RTDL changes from 1.88% + 0.00203% to 1.88% – 0.00203% for the 5.29 gram one, and their corresponding wavelength shifts are found by the curve fitting equation in Fig. 4. The differential of the two wavelength shifts corresponds with

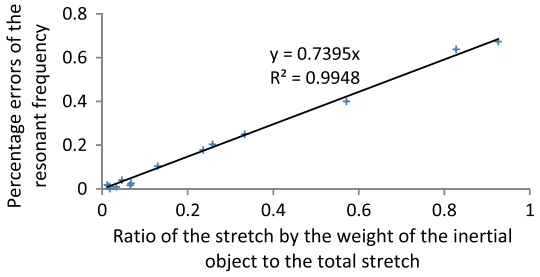

Fig. 13. Linear relationship found for modifying the resonant frequency.

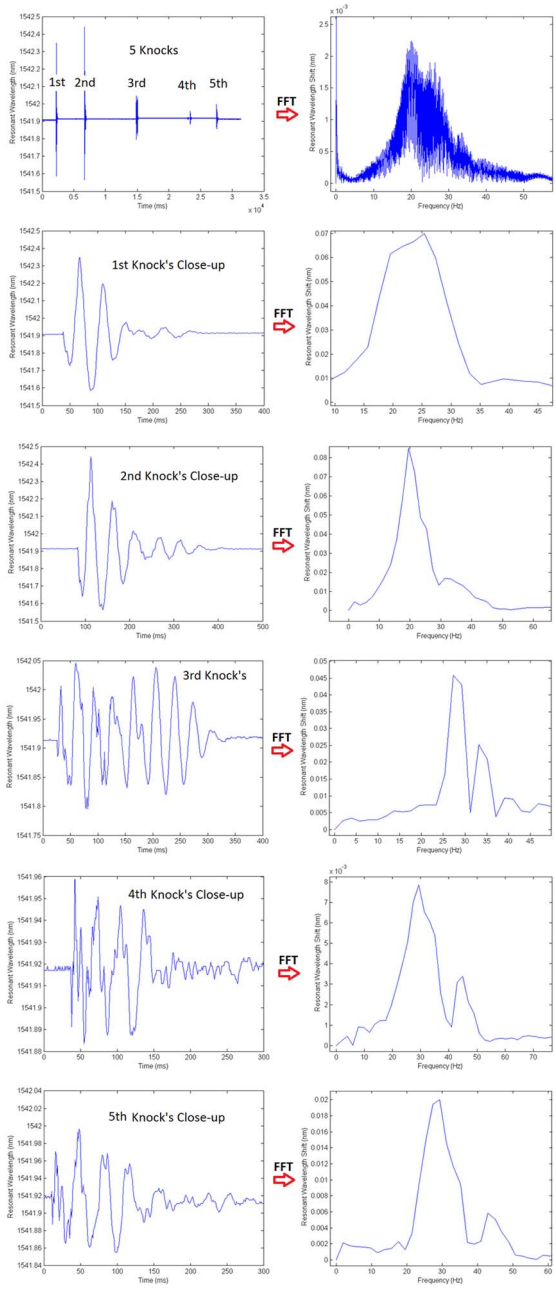

Fig. 14. Inconsistent resonant frequency records of the 5.29 gram accelerometer by the knock incitation method.

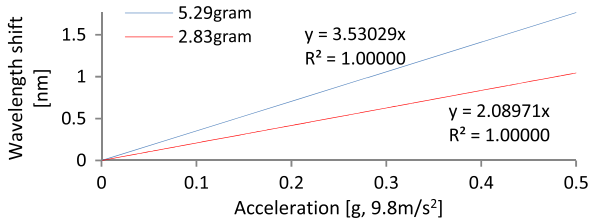

Fig. 15. Theoretical static sensitivities of the 5.29 and 2.83 gram accelerometers found by the classic method.

this acceleration at static. By increasing the assigned acceleration by 0.001 g each time, their static sensitivities are simulated and shown in Fig. 15.

When the FBG has a dominant stretch by the weight of the inertial object, the theoretical static sensitivity can be calculated by converting the assigned acceleration to the transverse force rather than RTDL. After all, at static, the measured acceleration of any accelerometer must be the same as the measurand. First, the transverse force at equilibrium is found, $0.00529 * 9.8$ N for the 5.29 gram one. Second, at 0.001 g, the force changes from $0.00529 * (9.8 + 0.001)$ N to $0.00529 * (9.8 - 0.001)$ N, and their corresponding wavelength shifts are found based on Fig. 16, which is achieved by a similar numerical simulation method as above [24]. The differential of these two wavelength shifts corresponds with this acceleration. By increasing the assigned acceleration by 0.001 g each time, its static sensitivity is simulated and is shown in Fig. 17. To show the influence of the prestretch on its sensitivity, the sensitivities are also simulated as if its prestretch were 0 and 0.4 nm. The fact shown in Fig. 17 that they overlap each other shows that a small prestretch scarcely influences the acceleration sensitivity, although it influences the force sensitivity heavily as shown in Fig. 16. By this method, the theoretical static sensitivities are found as 1.188 nm/g for the 5.29 gram one and 0.784 nm/g for the 2.83 gram one.

To test the over-range protection, the central cylinder of the 5.29 gram one was pulled by hands to each side of its shell three times, and Fig. 18 shows its records. Then, it was tested at 25 Hz, 5 g by a calibrated IMI 608A11 accelerometer (sensitivity 0.1 V/g, measurement range [–50 g, +50 g], and working at 1000 Hz), and Fig. 19 shows its records. The maximum wavelength shift was about 6.2 nm in both, which agrees with the theoretical value of 6.5 nm, because the transverse deflection is about

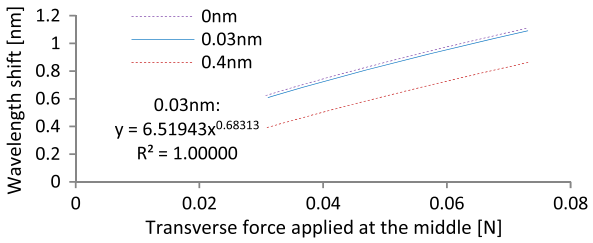

Fig. 16. Relations between an FBG's resonant wavelength shift and its subjected transverse force at its different prestretches.

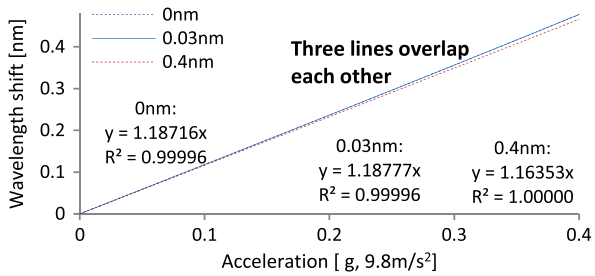

Fig. 17. Theoretical static sensitivity of the 5.29 gram accelerometer.

$((21 - 15)/2) - (1/2) + (0.3/2) = 2.65$ mm (taking the diameter of the unstripped fiber as 0.3 mm) and RTDL is 2.65/50 and corresponds with 6.5 nm based on Fig. 4.

The cross axial sensitivities of the two FBG accelerometers were tested in the other two orthogonal directions at 0.1 g, 5 Hz, and 0.4 g from 10 to 35 Hz.

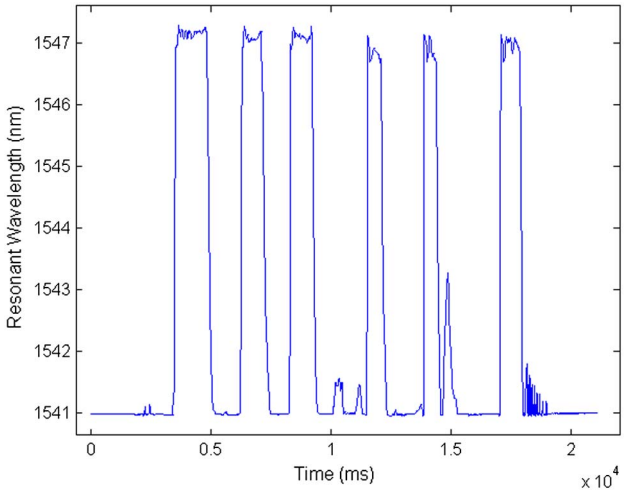

Fig. 18. Over-range protection experiment records of the 5.29 gram accelerometer when its central cylinder was pulled by hand to each side of its shell three times.

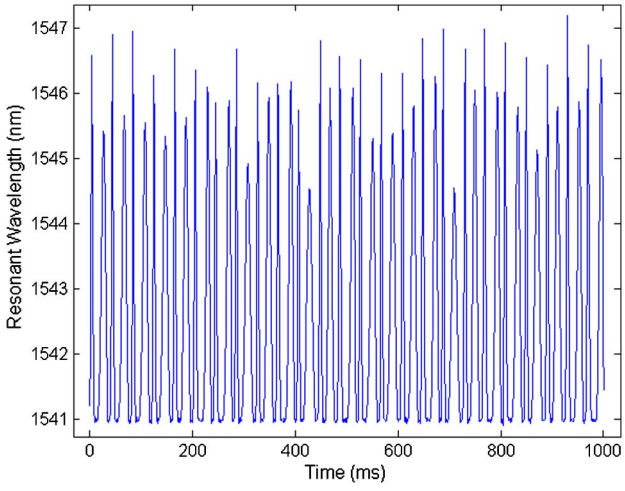

Fig. 19. Over-range protection experiment records of the 5.29 gram accelerometer at 25 Hz, 5 g.

Their resonant wavelength shifts were no more than 0.004 nm.

4. Conclusion

We demonstrate an FBG accelerometer with a high linear sensitivity, easy over-range protection, and low cross axial sensitivities by using transverse forces. The theoretical resonant frequency can be modified by the linear relationship between the percentage error of the resonant frequency and the ratio of the stretch by the weight of the inertial object to the total stretch, and the static sensitivity can be calculated by converting the assigned small, increasing acceleration to the transverse force rather than RTDL.

K. Li, M. H. Yau, and T. Nguyen acknowledge the doctorate scholarships provided by Queensland University of Technology. This work was also supported by the grants from the Research Grants Council of the Hong Kong SAR, China (RGC Ref No. 512006). We thank QUT staff William Gordon and Armin Liebhardt for their help in modeling and manufacturing the metal packages of the FBG accelerometers; Craig Cowled and Les King for their help in setting up the piezo accelerometer; Lincoln Hudson, Nathaniel Raup, and Len Wilcox for their help in experiments; and Micron Optics Ltd. technician Andrew Peterson for his help in configuring the FBG interrogator. K. Li proposed the idea, did the experiments, and drafted the paper; T. H. T. Chan, D. P. Thambiratnam, and H. Y. Tam supervised and coordinated the project; M. H. Yau prepared the FBG; and T. Nguyen assisted in the experiments.

References

1. D. Graham-Rowe, "Sensors take the strain," Nat. Photonics **1**, 307–309 (2007).
2. M. Jones, "Structural-health monitoring: a sensitive issue," Nat. Photonics **2**, 153–154 (2008).
3. A. Laudati, F. Mennella, M. Giordano, G. D'Altrui, C. C. Tassini, and A. Cusano, "A fiber-optic Bragg grating seismic sensor," IEEE Photon. Technol. Lett. **19**, 1991–1993 (2007).
4. Y. Zhang, S. Li, Z. Yin, B. Chen, H.-L. Cui, and J. Ning, "Fiber-Bragg-grating-based seismic geophone for oil/gas prospecting," Opt. Eng. **45**, 084404 (2006).
5. B. Lee, "Review of the present status of optical fiber sensors," Opt. Fiber Technol. **9**, 57–79 (2003).
6. T. A. Berkoff and A. D. Kersey, "Experimental demonstration of a fiber Bragg grating accelerometer," IEEE Photon. Technol. Lett. **8**, 1677–1679 (1996).
7. M. D. Todd, G. A. Johnson, B. A. Althouse, and S. T. Vohra, "Flexural beam-based fiber Bragg grating accelerometers," IEEE Photon. Technol. Lett. **10**, 1605–1607 (1998).
8. S. R. K. Morikawa, A. S. Ribeiro, R. D. Regazzi, L. C. G. Valente, and A. M. B. Braga, "Triaxial Bragg grating accelerometer," in *OFS 2002: 15th Optical Fiber Sensors Conference*, Technical Digest (2002), pp. 95–98.
9. J. N. C. Baldwin, J. Kiddy, and T. Salter, "Review of fiber optic accelerometers," in *23rd Conference and Exposition on Structural Dynamics 2005* (IMAC XXIII), Orlando, Florida, January 31–February 3, 2005.
10. J. H. Zhang, X. G. Qiao, M. L. Hu, Z. Y. Feng, H. Gao, Y. Yang, and R. Zhou, "Flextensional fiber Bragg grating-based accelerometer for low frequency vibration measurement," Chin. Opt. Lett. **9**, 090607 (2011).
11. A. Stefani, S. Andresen, W. Yuan, N. Herholdt-Rasmussen, and O. Bang, "High sensitivity polymer optical fiber-Bragg-grating-based accelerometer," IEEE Photon. Technol. Lett. **24**, 763–765 (2012).
12. Q. P. Liu, X. G. Qiao, J. L. Zhao, Z. A. Jia, H. Gao, and M. Shao, "Novel fiber Bragg grating accelerometer based on diaphragm," IEEE Sens. J. **12**, 3000–3004 (2012).
13. P. F. C. Antunes, C. A. Marques, H. Varum, and P. S. Andre, "Biaxial optical accelerometer and high-angle inclinometer with temperature and cross-axis insensitivity," IEEE Sens. J. **12**, 2399–2406 (2012).
14. P. Antunes, H. Varum, and P. S. Andre, "Uniaxial fiber Bragg grating accelerometer system with temperature and cross axis insensitivity," Measurement **44**, 55–59 (2011).
15. Y. X. Guo, D. S. Zhang, H. Meng, X. Y. Wen, and Z. D. Zhou, "Metal packaged fiber Bragg grating accelerometer," Proc. SPIE **8421**, 84213V (2012).
16. N. Basumallick, I. Chatterjee, P. Biswas, K. Dasgupta, and S. Bandyopadhyay, "Fiber Bragg grating accelerometer with enhanced sensitivity," Sens. Actuators A **173**, 108–115 (2012).
17. J. Zhang, X. Qiao, M. Hu, Z. Feng, H. Gao, Y. Yang, and R. Zhou, "Proposal of metal bellows-based fiber Bragg grating accelerometer," Chin. Opt. Lett. **9**, 090606 (2011).
18. K. Li and Z. A. Zhou, "A high sensitive fiber Bragg grating strain sensor with automatic temperature compensation," Chin. Opt. Lett. **7**, 191–193 (2009).
19. Y. L. Yu, H. Y. Tam, W. H. Chung, and M. S. Demokan, "Fiber Bragg grating sensor for simultaneous measurement of displacement and temperature," Opt. Lett. **25**, 1141–1143 (2000).
20. H. Y. Au, S. K. Khijwania, H. Y. Fu, W. H. Chung, and H. Y. Tam, "Temperature-insensitive fiber Bragg grating based tilt sensor with large dynamic range," J. Lightwave Technol. **29**, 1714–1720 (2011).
21. R. Aneesh, M. Maharana, P. Munendhar, H. Y. Tam, and S. K. Khijwania, "Simple temperature insensitive fiber Bragg grating based tilt sensor with enhanced tunability," Appl. Opt. **50**, E172–E176 (2011).
22. J. Jung, H. Nam, B. Lee, J. O. Byun, and N. S. Kim, "Fiber Bragg grating temperature sensor with controllable sensitivity," Appl. Opt. **38**, 2752–2754 (1999).
23. K. Li, Z. A. Zhou, and A. Liu, "A high sensitive fiber Bragg grating cryogenic temperature sensor," Chin. Opt. Lett. **7**, 121–123 (2009).
24. K. Li, M. H. Yau, T. H. T. Chan, D. Thambiratnam, and H. Y. Tam, "Fiber Bragg grating strain modulation based on nonlinear string transverse-force amplifier," Opt. Lett. **38**, 311–313 (2013).
25. P. L. Walter, "The history of the accelerometer," J. Sound Vib. **31**, 16–22 (1997).
26. IMI Sensors, "Model 626B02," www.imi-sensors.com/Industrial_Accelerometers/Low_Frequency/626B02.aspx.
27. P. Touboul, B. Foulon, and E. Willemenot, "Electrostatic space accelerometers for present and future missions," Acta Astronaut. **45**, 605–617 (1999).
28. D. E. Weiss, "Design and application of accelerometers," *Proc. SESA (now SEM)* (Addison-Wesley, 1947), Vol. **IV**, pp. 89–99.